Published in final edited form as:
Biochemistry. 2010 August 10; 49(31): 6617–6626. doi:10.1021/bi100490u.

Elucidation of the Functional Metal Binding Profile of a Cd^{II}/Pb^{II} sensor $CmtR^{Sc}$ from *Streptomyces coelicolor*

Yun Wang[‡,1], **John Kendall**[§], **Jennifer S. Cavet**[§,2], and **David P. Giedroc**[‡,¶,2]

[‡]Department of Biochemistry and Biophysics, Texas A&M University, College Station, TX 77843-2128

[§]Faculty of Life Sciences, University of Manchester, Manchester, UK

[¶]Department of Chemistry, Indiana University, Bloomington, IN 47405-7102

Abstract

Metal homeostasis and resistance in bacteria is maintained by a panel of metal sensing transcriptional regulators that collectively control transition metal availability and mediate resistance to heavy metal xenobiotics, including As^{III}, Cd^{II}, Pb^{II} and Hg^{II}. The ArsR family constitutes a superfamily of metal sensors that appear to conform to the same winged helical, homodimeric fold, that collectively "sense" a wide array of beneficial metal ions and heavy metal pollutants. The genomes of many actinomycetes, including the soil dwelling bacterium *Streptomyces coelicolor* and the human pathogen *Mycobacterium tuberculosis*, encode over ten ArsR family regulators, most of unknown function. Here, we present the characterization of a homolog of *M. tuberculosis* CmtR ($CmtR^{Mtb}$) from *S. coelicolor*, denoted $CmtR^{Sc}$. We show that $CmtR^{Sc}$, in contrast to $CmtR^{Mtb}$ binds two monomer mol equivalents of Pb^{II} or Cd^{II} to form two pairs of trigonal S_3 coordination complexes per dimer. Metal site 1 conforms exactly to the α4C site previously characterized in $CmtR^{Mtb}$ while metal site 2 is coordinated by a C-terminal vicinal thiolate pair, Cys110 and Cys111. Biological assays reveal that only Cd^{II} and, to a lesser extent, Pb^{II} mediate transcriptional derepression in the heterologous host *M. smegmatis* in a way that requires metal site 1. In contrast, mutagenesis of metal site 2 ligands Cys110 or Cys111 significantly reduces Cd^{II} responsiveness, with no detectable effect on Pb^{II} sensing. The implications of these findings on the ability to predict metal specificity and function from metal-site "signatures" in the primary structure of ArsR family proteins are discussed.

The concentrations of first-row *d*-block transition metal ions and other heavier, toxic di- and trivalent metal ions and metalloids that play no biological role can vary dramatically in the immediate environment of a bacterial community. Although some are essential, and enable proteins to adopt their native three-dimensional structures or function as cofactors for metalloenzyme catalysis, an excess beyond that required by normal cellular metabolism can also be strongly deleterious to cell viability (1). As a result, metal-specific regulatory systems have evolved that detect metal-sufficiency or toxicity and control the intracellular availability of the different metal ions as well as purge any toxic elements or compounds from the cytosol. In free-living microorganisms, such detoxification/resistance systems are particularly important because it permits these organisms to survive by adaptation to potentially harsh environmental conditions, e.g., soil and water heavily contaminated by

[2]To whom correspondence should be addressed: For J. S. C., Life Sciences, Michael Smith Building, University of Manchester, Oxford Road, Manchester M13 9PT, UK. Tel.: +44 161 275 51543; Fax: +44 161 275 5082; jennifer.s.cavet@manchester.ac.uk. For D. P. G., Department of Chemistry, Indiana University, Simon Hall 320A, 212 S. Hawthorne Drive, Bloomington, IN 47405-7102. Tel: 812-856-3178; Fax: 812-856-5710; giedroc@indiana.edu..
[1]Present address for Y. W.: Division of Medicinal Chemistry, College of Pharmacy, The University of Texas, Austin, Texas 78712

heavy metal salts (2) and/or the phagosome of mammalian host cells for certain microbial pathogens (3). Large, highly polarizable and thiophilic metal ions such as Hg^{II}, Cd^{II} and Pb^{II} are highly toxic, in part because they are capable of forming high affinity, kinetically long-lived complexes with protein cysteine thiolates found in native zinc binding sites, thereby rendering them nonfunctional. Such proteins include canonical zinc finger proteins and 5-aminolevulinic acid dehydratase (ALAD) in mammals (4,5).

CmtR is a Cd^{II} sensing SmtB/ArsR (or ArsR) family metalloregulatory repressor from *Mycobacterium tuberculosis* (6–9). In addition to Cd^{II}, *M. tuberculosis* CmtR (denoted $CmtR^{Mtb}$ here) senses Pb^{II} in the heterologous host *M. smegmatis* and has been shown to form Cys-thiolate rich metal coordination complexes with Cd^{II}, Pb^{II} and even Zn^{II} *in vitro* (6,7). CmtR possesses a unique pair of α4C metal binding sites (metal ligands derived from the α4 helix and the C-terminal tail; see Fig. 1B) (6,8,10,11) structurally distinct from the Cd^{II}/Pb^{II} sites of another SmtB/ArsR Cd^{II}/Pb^{II} sensor, *Staphylococcus aureus* plasmid pI258-encoded CadC, which contains functional α3N and nonfunctional α5 metal sites (1,12,13). The solution structure of the CmtR-Cd^{II} complex reveals a homodimer with metal bound to Cys102' from the C-terminal tail region of one subunit and Cys57, Cys61 in the helix α4 from the other subunit; Pb^{II} is predicted to bind to the same pair of sites (7,8) (Fig. 1). Cys102 plays an accessory role in stabilizing the coordination complex while Cys57 and Cys61 anchor it, contributing most of the metal binding affinity (7). However, Cys102 does function as a key allosteric metal ligand in mediating the disassembly of oligomeric CmtR-*cmt* O/P1 oligomeric complexes *in vitro* (7,8), and for derepression *in vivo* (6), although the structural and dynamic changes induced in the dimer upon Cys-102 Cd^{II} binding remain to be characterized.

Recent *in vivo* experiments using *M. tuberculosis* suggest that $CmtR^{Mtb}$ binds cooperatively to four binding sites in an extended 90-bp region upstream of the *cmtR-Rv1993c-cmtA* operon, to inhibit the interaction of RNA polymerase with the promoter region (9). These studies also suggest that Cd^{II} is the sole inducer in *M. tuberculosis*, a situation that contrasts with findings in the heterologous host, *M. smegmatis* (6,9). The *cmtA* gene encodes a deduced metal transporting P_{1B}-ATPase efflux pump, which is proposed to efflux toxic metal ions from the bacterial cytosol (6,9). Therefore, increasing cellular Cd^{II} concentration triggers derepression of the *cmtR-Rv1993c-cmtA* operon, resulting in increased concentrations of CmtA in the plasma membrane which is thought to export Cd^{II} from the cytosol against a metal concentration gradient (9).

Streptomyces coelicolor A3(2) is representative of a ubiquitous group of soil-dwelling, filamentous Gram-positive bacteria. This highly adaptable organism undergoes a broad range of metabolic processes and biotransformations, and is noted for its natural antibiotic production (14). Like *M. tuberculosis*, *S. coelicolor* belongs to the taxonomy order of *Actinomycetales* (14,15). Although each has very different lifestyles, both encode elaborate metal detoxification and efflux systems. As a human pathogen, *M. tuberculosis* must adapt to various microenvironmental niches, including the phagosome of infected macrophages where it encounters changes in metal availability (3,16–19). *S. coelicolor* must also sense and respond to fluctuating metal levels within soils (20–22). Notably, the sequenced strains of *M. tuberculosis* and *S. coelicolor* possess multiple deduced ArsR family regulators, ten (10) and fourteen, respectively, as well as representatives of many of the other metalloregulatory protein classes (1,23). The diversity of the metal-responsive regulators in these two organisms is therefore likely to reflect their different ecological niches and the different survival strategies employed to avoid metal stress. A search for protein homologs of *M. tuberculosis* CmtR returned two open reading frames in *S. coelicolor* A3(2)

[1]Abbreviations used are: DTNB, 5,5'-dithiobis(2-nitrobenzoic acid); LMCT, ligand-to-metal charge transfer; O/P, operator/promoter.

corresponding to locus tags SCO0875 and SCO3522. The gene products of SCO0875 and SCO3522 possess only ten amino acid differences between them, and each shares ≈50% identity with *M. tuberculosis* CmtR. Both SCO0875 and SCO3522 are immediately upstream of deduced cation diffusion facilitator (CDF) family integral membrane metal transporters (Fig. 1A), with predicted roles in the transport of the more thiophilic metal ions (24). SCO0875 was chosen for detailed study herein and designated $CmtR^{Sc}$.

$CmtR^{Sc}$ shares four conserved cysteine residues with $CmtR^{Mtb}$ which include the three Cd^{II} ligands (Cys57, Cys61 and Cys102) required for metal binding and allosteric regulation (6) as well as C24 in the α2 helix (Fig. 1A). As a result, we expected to observe at least partially similar metal binding profiles for $CmtR^{Mtb}$ and $CmtR^{Sc}$. However, $CmtR^{Sc}$ contains two additional cysteines arranged as C-terminal vicinal pair (Cys110 and Cys111) that could also be involved in metal coordination (Fig. 1C). It was therefore of interest to functionally and structurally characterize $CmtR^{Sc}$ and compare its properties to that of $CmtR^{Mtb}$. We show here that the $CmtR^{Sc}$ homodimer harbors a second pair of high affinity Cys-thiolate rich Cd^{II}/Pb^{II} coordination sites relative to $CmtR^{Mtb}$ that involves metal coordination by Cys110 and Cys111. We further show that wild-type $CmtR^{Sc}$, is a *bona fide* CmtR that is highly selective for Cd^{II}/Pb^{II} in the heterologous host *M. smegmatis*, the same host used to characterize $CmtR^{Mtb}$, with no other metal ions, including Hg^{II} and Zn^{II}, capable of inducing transcriptional derepression. Strikingly, the second pair of Cd^{II}/Pb^{II} sites unique to $CmtR^{Sc}$ is required for full Cd^{II}-responsiveness in *M. smegmatis*, but does not alter Pb^{II} sensing under the same conditions. The structural and functional implications of these findings for the prediction of metal-sensing sites in ArsR family metal sensors are discussed.

MATERIALS AND METHODS

Construction of wild-type and C110G/C111S $CmtR^{Sc}$ overexpression plasmids

To create pET3a-$CmtR^{Sc}$, the $CmtR^{Sc}$ coding region was amplified by PCR from *Streptomyces violaceoruber* genomic DNA (M145, used in to sequence the *S. coelicolor* genome (14) using primers V (5'-AAAAACATATGGTGCTGACTCTCGCTGCCGATATC-3') and VI (5'-AAAAAGCTAAGCTCAGCAGCACTCCTTCTCGTC-3') and cloned into pET3a (Novagen) between the *Nde*I and *BPU1102*I restriction sites using standard methods. The plasmid encoding C110G/C111S $CmtR^{Sc}$ was generated by site-directed mutagenesis using the QuikChange kit (Stratagene) and primers VII (5'-GGACGAGAAGGAGGGCTCCTGAGCAATAACTAGC-3') and primer VIII (5'-GCTAGTTATTGCTCAGGAGCCCTCCTTCTCGTCC-3') using pET3a-$CmtR^{Sc}$ as the template. The integrity of all expression plasmids was verified by DNA sequencing.

Purification of wild type and mutant $CmtR^{Sc}$

$CmtR^{Sc}$ and C110G/C111S $CmtR^{Sc}$ were purified to homogeneity using a procedure previously described for $CmtR^{Mtb}$ (7). The theoretical molecular weight for $CmtR^{Sc}$ is 12.2 kDa and the extinction coefficient was calculated to be 3730 $M^{-1}\bullet cm^{-1}$.

Free thiol determination

A standard DTNB1 colorimetric assay was used to determine the number of free thiols in $CmtR^{Sc}$ (25). 25 μL 2.5 mM DTNB solution was added separately into 400 μL 10–15 μM protein. After a 30 min incubation in the anaerobic chamber, the concentration of thiolate anion was quantified at 412 nm (ε=13,600 $M^{-1}\bullet cm^{-1}$) after subtraction of the absorbance of the final dialysis buffer with same concentration of DTNB. The number of free thiols in wild-type $CmtR^{Sc}$ was 5.8 ± 0.2 (6 expected) and 3.0 ± 0.2 (4 expected) for C110G/C111S $CmtR^{Sc}$.

Atomic absorption spectroscopy

The concentrations of all metal titrants were determined using a Perkin-Elmer Analyst 700 atomic absorption spectrophotometer operating in flame mode using a different hollow cathode lamps specific for each metal (25). Zn^{II} was detected at 213.9 nm (slit=0.7 nm), Cd^{II} was detected at 228.8 nm (slit = 0.7 nm) and Pb^{II} was detected at 283.3 nm (slit = 0.7 nm).

Analytical Sedimentation Equilibrium Ultracentrifugation

All experiments were carried out on a Beckman Optima XL-A analytical ultracentrifuge with the rotor speed set to 20,000 rpm at 25.0 °C. Ultracentrifuge cells were assembled in the anaerobic glove box and contained 5.0 μM $CmtR^{Sc}$ wild-type or 8.0 μM C110G/C111S $CmtR^{Sc}$ in buffer (10 mM Hepes, 0.4 M NaCl, and 0.1 mM EDTA at pH 7.0). Scans were monitored by absorbance at 232 nm or 233 nm for the wild-type and C110G/C111S $CmtR^{Sc}$, respectively, with the final seven scans extracted and subjected to simultaneous fitting using Ultrascan II 8.0. A partial specific volume (ν) of 0.7354 ml/g (predicted by Sednterp 1.07 software, www.bbri.org/RASMB/rasmb.html) and a buffer density (ρ) of 1.0 g/ml were used in the analysis. The data were globally and simultaneously fitted to either a one component ideal species model or a monomer-dimer equilibrium model using eqs. 1 and 2, respectively:

$$C(\mathrm{X}) = e^{\left[\frac{\ln(A)+M\omega^2\left(1-\bar{\nu}\rho\right)\left(X^2-X_r^2\right)}{2RT}\right]}+B \qquad \text{(Eq. 1)}$$

$$C(\mathrm{X}) = e^{\left[\frac{2\ln(A)+\ln\left(\frac{2}{EL}\right)+\ln\left(K_{1,2}\right)+2M\omega^2\left(1-\bar{\nu}\rho\right)\left(X^2-X_r^2\right)}{2RT}\right]}+e^{\left[\frac{\ln(A)+M\omega^2\left(1-\bar{\nu}\rho\right)\left(X^2-X_r^2\right)}{2RT}\right]}+B \qquad \text{(Eq. 2)}$$

where X = cell radius, X_r = reference radius, A = amplitude of monomer*, M = molecular weight of monomer*, E = extinction coefficient, R = gas constant, T = temperature, B = baseline offset*, ω = angular velocity, L = optical pathlength, $K_{1,2}$ = monomer–dimer equilibrium constant*, and * indicates this parameter can be floated during parameter optimization (26). Fits to the monomer-dimer model did not significantly improve the goodness-of-fit, consistent with a low concentration of monomeric species under these solution conditions; thus, $K_{1,2} \geq 10^6\ \mathrm{M}^{-1}$.

Cd^{II}, Pb^{II} optical absorption spectroscopy

All metal binding experiments were carried out anaerobically at ambient temperature (~25°C) using a Hewlett-Packard model 8452A spectrophotometer (12,27). For Cd^{II} titrations, apo proteins were diluted using final dialysis buffer S to ≈ 50 μM in 800 μL and loaded into an anaerobic cuvette fitted with a Hamilton gas-tight adjustable volume syringe containing 0.5 mM Cd^{II} titrant in the glove box. Complete optical spectra of apo protein were collected from 200–900 nm 1–2 min after each addition of a known aliquot (5–15 μL) of Cd^{II}. Corrected spectra were obtained by subtraction of the apo protein spectra from each spectrum obtained after addition of metal ion, and further corrected for dilution. Pb^{II} titrations were done in exactly the same way except that 10 mM bis-Tris, 0.4 M NaCl, pH 7.0 was used as the buffer. Bis-Tris is a weakly chelating buffer that can prevent excess Pb^{II} from forming $Pb^{II}(OH)_2$ precipitate (4). Cd^{II} competition experiment performed with EDTA was carried out as described above except 200–300 μM chelator was present. The competition binding curves were fit to the model using Dynafit:

$$P+Cd \leftrightarrows P.Cd, K_{Cd1};$$

$$P.Cd+Cd \leftrightarrows P.Cd2, K_{Cd2};$$

$$EDTA+Cd \leftrightarrows EDTA.Cd, K_{Cd-EDTA}$$

where P is the monomer concentration of CmtR^{Sc} and $K_{Cd\text{-}EDTA}$ (pH 7.0) = 8.31×10^{13} M^{-1} under these conditions using a pH-dependent log K_{Cd}=16.5 and pK_as of 9.52 and 6.13 for EDTA (28).

Zn^{II} binding experiments

The zinc chelator dye magfura-2 ($K_{Zn} = 5.0 \times 10^7$ M^{-1} at pH 7.0 and 25°C) was used as a colorimetric competitor for Zn^{II} binding by wild-type and C110G/C111S CmtR^{Sc} as previously described (29). 30 μM CmtR^{Sc} and ≈15 μM magfura-2 was used for all experiments. The data were fit to a competitive binding model assuming two nonequivalent, noninteracting metal binding sites per CmtR^{Sc} protomer for CmtR^{Sc} wild-type by DynaFit:

$$P+Zn \leftrightarrows P-Zn, K_{PZn};$$

$$P.Zn+Zn \leftrightarrows P-Zn_2, K_{PZn2};$$

$$magfura\_2+Zn \leftrightarrows magfura\_2-Zn,$$

where $K_{Zn\text{-}magfura2} = 5.0 \times 10^7$ M^{-1} under these conditions. For C110G/C111S CmtR^{Sc}, data were fitted as above to a competitive binding model assuming one metal binding site per protomer or two per dimer (without K_{PZn2}).

Construction of promoter-lacZ fusions, site-directed mutagenesis and β-galactosidase assays

CmtR^{Sc} upstream sequences and the coding region (539 bp) were amplified from *S. coelicolor* genomic DNA using primers 5'-GAAAGTACTGCGGGTAGTGGCGATGTGATCC-3' and 5'-GAAGGTACCGCGGTCATTCAGCAGC-3', and ligated to pGEM-T prior to subcloning into the *Sca*I/*Kpn*I site of pJEM15 (30) to create a transcriptional fusion with *lacZ*. QuickChange XL (Stratagene) site-directed mutagenesis was subsequently employed to generate derivatives with the following codon substitutions in CmtR^{Sc}: Cys24, Cys57, Cys61, Cys102, Cys110, and Cys111, each to Ser; and Arg16 to a UGA stop codon. All generated plasmid constructs were checked by sequence analysis. *Mycobacterium smegmatis* mc^{2}155 was used as an actinomycete host for reporter gene assays. The *lacZ* fusion constructs were introduced into *M. smegmatis* and transformants selected on Luria-Bertani (LB) agar supplemented with 25 μg mL^{-1} kanamycin as described previously (30). β-galactosidase assays were performed as described (31) in triplicate on at least three separate occasions. Cells were grown at 37 °C with shaking in LB broth or Sauton medium

containing 0.05% (v/v) Tween 80 and kanamycin (25 μg ml^{-1}) supplemented with the indicated concentration of metal salt (described in individual experiments) for ~20 h immediately prior to assays. The metal salts used were $ZnSO_4$, $CoSO_4$, $NiCl_2$, $CdCl_2$, $Pb(C_2H_3O_2)_2$, $CuSO_4$, $AsNaO_2$ and $HgCl_2$.

RESULTS

Wild-type and C110G/C111S $CmtR^{Sc}$ are stable homodimers at low protein concentrations

Both $CmtR^{Sc}$ and its C110G/C111S mutant were subjected to analytical equilibrium sedimentation ultracentrifugation at 20,000 rpm at 5 μM and 8 μM monomer concentration, respectively, and absorbance recorded at 232 nm, with representative results shown in Fig. 2. Each set of experimental data that had reached equilibrium was first subjected to a global simultaneous fit to a single ideal species model indicated by a solid line. The apparent molecular weights obtained from these data (Fig. 2) are consistent with both apo-$CmtR^{Sc}$ and apo-C110G/C111S $CmtR^{Sc}$ being predominantly homodimeric under these conditions.

$CmtR^{Sc}$ possesses two Cd^{II} binding sites per monomer while C110G/C111S $CmtR^{Sc}$ possesses one

Apoprotein-subtracted Cd^{II} absorbance spectra of $CmtR^{Sc}$ are shown in Fig. 3. The saturated Cd^{II} spectra is characterized by an intense ligand-to-metal charge transfer (LMCT1) at 240 nm, similar to that observed for $CmtR^{Mtb}$ (7). Binding isotherms (*insets*) were obtained by plotting the corrected absorbance at 240 nm as a function of total [Cd^{II}] over protein monomer ratio. The maximum molar absorptivity at 240 nm for $CmtR^{Sc}$ is ≈ 31,000 M $(monomer)^{-1}$ cm^{-1} which is two-fold larger than wild-type mycobacterial $CmtR^{Mtb}$ (ε ≈ 16,000 M^{-1} cm^{-1}) (Fig. 3A) (7). In addition, $CmtR^{Sc}$ exhibits a 2:1 (Cd^{II}:$CmtR^{Sc}$ monomer) binding stoichiometry (Fig. 3A), in contrast to $CmtR^{Mtb}$ which is known to bind one metal per protomer (7). Nonlinear least-squares fits of the binding isotherms to a simple 2:1 independent-site metal binding model returns only a lower limit of the binding affinity given the stoichiometric nature of these binding curves ($K_{Cd} > \approx 5 \times 10^7$ M^{-1}) (Fig. 3A).

The presence of an additional Cd^{II} site in the $CmtR^{Sc}$ homodimer coupled with twice the Cys $S^- \rightarrow Cd^{II}$ molar absorptivity prompted us to investigate if the two vicinal cysteine residues (Cys110 and Cys111) at the C-terminus donate thiolate ligands to the second Cd^{II} ion. We measured the Cd^{II} absorption spectrum of C110G/C111S $CmtR^{Sc}$, where the two C-terminal cysteines were converted to their analogous residues in $CmtR^{Mtb}$ (Fig. 1C). As expected, C110G/C111S $CmtR^{Sc}$ behaves much like $CmtR^{Mtb}$, given a ≈0.9:1 Cd^{II}:C110G/C111S monomer stoichiometry and an identical monomer molar absorptivity of ≈ 16,000 M^{-1} cm^{-1} (Fig. 3B) (7), which is precisely half that of wild-type $CmtR^{Sc}$. As expected, the binding of Cd^{II} is stoichiometric under these conditions and thus returns only a lower limit of the metal binding affinity (Fig. 3B). Given a molar absorptivity of ≈5500 M^{-1} cm^{-1} per Cd-S coordination bond (32–34), it is reasonable to conclude that C110G/C111S $CmtR^{Sc}$ possesses one Cd^{II} site (termed metal site 1) that is identical to the previously characterized canonical α4C site $CmtR^{Mtb}$, while wild-type $CmtR^{Sc}$ possesses two spectroscopically similar Cd^{II} binding sites (metal sites 1 and 2).

The Cd^{II} affinities of each metal site per monomer in wild-type $CmtR^{Sc}$ were estimated by carrying out a Cd^{II} titration experiment in the presence of a known concentration of the metal chelator EDTA (Fig. 3*C*), with $K_{Cd\text{-}EDTA} = 8.3 \times 10^{13}$ M^{-1} under these solution conditions (pH 7.0, 25.0 °C). A nonlinear least squares fit of a simple competition model assuming two non-equivalent, non-interacting sites per protomer gives $K_{Cd1} = 3.0\ (\pm 0.1) \times 10^{13}$ M^{-1}, $K_{Cd2} = 3.6\ (\pm 0.5) \times 10^{12}$ M^{-1}. These data taken together confirm that $CmtR^{Sc}$ has two pairs of structurally similar high affinity metal sites per homodimer, which differ in

macroscopic affinity by ≈10-fold. Previous findings with $CmtR^{Mtb}$ reveal that Cys57, Cys61 and Cys102 are ligands to Cd^{II} and form trigonal pyramidal coordination geometry (S_3) or distorted tetrahedral coordination geometries (S_3O), with Cys102 not as strongly bound as the other thiolate ligands (6–8) (see Fig. 1B). Considering these three cysteines are conserved in $CmtR^{Mtb}$ and $CmtR^{Sc}$, they likely create a Cd^{II} site indistinguishable to that in $CmtR^{Mtb}$ and is denoted metal site 1. In contrast, Cd^{II} site 2 clearly requires coordination by Cys110 and Cys111.

$CmtR^{Sc}$ possesses two Pb^{II} binding sites and the same C110G/C111S mutation abolishes one

Anaerobic Pb^{II} titration experiments were performed using ≈50 μM apo-wild-type $CmtR^{Sc}$ (Fig. 4A) and C110G/C111S $CmtR^{Sc}$ (Fig. 4B) and the apoprotein-subtracted difference spectra are shown. The saturated Pb^{II} spectra of both proteins are characterized by an intense absorption in the far-ultraviolet and a long-wavelength absorption band with maximum at 333 nm, identical to that of $CmtR^{Mtb}$ (7) and report on ligand-to-metal charge transfer (S^- 3p→Pb 6p) and intraatomic (Pb $6s^2$→Pb 6sp) electronic transitions (35,36). Binding isotherms (*insets*) were obtained by plotting the corrected absorbance at 333 nm as a function of total [Pb^{II}]/protein monomer ratio. As expected, for wild-type $CmtR^{Sc}$ Pb^{II} binding is saturable at ≈ 2:1 ratio over [$CmtR^{Sc}$] monomer (Fig. 4A); in contrast, this stoichiometry drops to ≈ 0.7 Pb^{II}/monomer for C110G/C111S $CmtR^{Sc}$ (Fig. 4B). These Pb^{II} stoichiometries are largely consistent with the relative monomer molar absorptivities at 333 nm (ε_{333}) of ≈7900 M^{-1} cm^{-1} and ≈3950 M^{-1} cm^{-1} for wild-type $CmtR^{Sc}$ and C110G/C111S $CmtR^{Sc}$, respectively (Fig. 4). Interestingly, the Pb^{II}-thiolate molar absorptivity of C110G/C111S $CmtR^{Sc}$ appears to be about one-half that of $CmtR^{Mtb}$ (7) for reasons that are not clear, although the fractional stoichiometries in each case may complicate this. Furthermore, unlike for Cd^{II}-binding, the extent to which molar absorption wavelength and intensity reports on coordination number and geometry for Pb^{II}-thiolate complexes has not yet been firmly established (12,36–39). In any case, the simplest conclusion is that substitution of Cys110 and Cys111 with non-liganding residues abolishes Pb^{II} binding to metal site 2, as is the case for Cd^{II}.

$CmtR^{Sc}$ binds two Zn^{II} per monomer as determined by chelator competition experiments with magfura-2

The zinc indicator dye magfura-2 ($K_{Zn•mag\text{-}fura\text{-}2} = 5.0 \times 10^7$ M^-) was used as a competitor of Zn^{II} binding to $CmtR^{Sc}$ and the C110G/C111S mutant to determine the Zn^{II} binding stoichiometry and affinity constant K_{Zn} (11). Figure 5 shows representative titrations of Zn^{II} into mixtures of wild-type $CmtR^{Sc}$ (Fig. 5A) and C110G/C111S $CmtR^{Sc}$ (Fig. 5B) and magfura-2. The solid curve represents a fit to a model that describes the binding of two Zn^{II} ions to the wild-type $CmtR^{Sc}$ monomer, considering each monomer-metal binding as an independent event (Fig. 5A). For wild-type $CmtR^{Sc}$, the estimated parameters are similar for both zinc ions, with $K_{PZn} = 5.3$ (±1.8) $\times 10^8$ M^- and $K_{PZn2} = 6.7$ (±1.4) $\times 10^8$ M^-. These binding affinities differ from that determined previously for the $CmtR^{Mtb}$ dimer, which showed strong negative cooperativity within the dimer with one site in ≈10^{10} M^- range and the other in ~10^5 M^{-1} range under the same solution conditions (7). For the C110G/C111S $CmtR^{Sc}$ mutant, competition titration curves were fit to a model that describes the binding of one Zn^{II} ion to the C110G/C111S $CmtR^{Sc}$ monomer (Fig. 5B), with an estimated affinity of $K_{PZn} = 5.5$ (±1.2) $\times 10^7$ M^{-1}.

Cadmium and lead alleviate $CmtR^{Sc}$ mediated repression

M. smegmatis mc^2155 was previously used to characterize $CmtR^{Mtb}$ and hence was exploited as a heterologous host for the characterization of $CmtR^{Sc}$, thereby allowing direct comparison of these two regulators within the same cytosol. *M. smegmatis* mc^2155 and *S.*

coelicolor are closely related actinomycetes, with similarly high GC-contents, and recognition of *Streptomyces* operator-promoter elements by the mycobacterial transcription machinery (40,41) has been exploited previously to characterize *S. coelicolor* genes *in vivo* (41). To determine which, if any, metals are sensed by $CmtR^{Sc}$ *in vivo*, a 539-bp DNA fragment including the $cmtR^{Sc}$ operator-promoter and coding region was fused to a promoterless *lacZ* in plasmid pJEM15 and introduced into *M. smegmatis* mc^2155. β-galactosidase activity was measured following growth (~20 h) of cells in medium supplemented with maximum permissive concentrations of various metals. At these biologically significant metal levels, elevated activity was detected in response to Cd^{II} and, to a lesser extent, Pb^{II} but no other metals (Fig. 6A). Furthermore, in the absence of added metal ions, elevated β-galactosidase activity was detected in cells containing an analogous construct in which codon-16 within the $cmtR^{Sc}$ coding region was converted to a stop codon (Fig. 6B), confirming that $CmtR^{Sc}$ acts negatively toward expression.

$CmtR^{Sc}$ senses Cd^{II} and Pb^{II} using α4C sites

The previously characterized Cd^{II} binding α4C sensing sites of $CmtR^{Mtb}$ involve Cys102 from the C-terminal region of one subunit in association with Cys57 and Cys61 from helix αR of the other subunit (6–8) (see Fig. 1B). Comparison of the amino acid sequences of $CmtR^{Sc}$ and related ArsR family sensors reveals that the α4C ligands are completely conserved in $CmtR^{Sc}$ and $CmtR^{Mtb}$, while $CmtR^{Sc}$ lacks residues corresponding to other previously defined ArsR family metal-binding motifs (1,10). Substitution of the α4C cysteines (Cys57, Cys61 and Cys102) in $CmtR^{Sc}$ with serines created functional repressors that mediated low expression of *lacZ* in cells grown with no metal supplement, but repression was not alleviated at Cd^{II} concentrations that caused loss of repression by wild-type $CmtR^{Sc}$ (Fig. 7A). In addition, no alleviation of repression was observed in the presence of maximum permissive concentrations of Pb^{II} (Fig. 7A). Hence, consistent with findings for $CmtR^{Mtb}$ (6), Cys57, Cys61 and Cys102 at α4C are obligatory for both Cd^{II} and Pb^{II} recognition by $CmtR^{Sc}$ *in vivo* and likely contribute toward a single common metal-binding site, metal site 1.

Cd^{II}, but not Pb^{II}, sensing by $CmtR^{Sc}$ involves an additional pair of C-terminal cysteines

As discussed above, in addition to Cys57, Cys61 and Cys102 at α4C, $CmtR^{Sc}$ possesses three further cysteines (Cys24 found in both CmtRs, and Cys110 and Cys111 which are unique to $CmtR^{Sc}$, Fig. 1C). In the absence of added Cd^{II} or Pb^{II}, β-galactosidase activity remained low in cells containing Ser substitutions of Cys24, Cys110 or Cys111, consistent with retention of repressor function (Fig. 7A). However, although inducer recognition was clearly retained in these cells, Cd^{II}-mediated derepression was substantially reduced in cells containing the single Cys110 and Cys111 substitution mutants (Fig. 7A). Indeed, when expression from the *cmtR* operator-promoter was examined in cells exposed to a range of Cd^{II} and Pb^{II} concentrations, Cd^{II}-responsiveness was significantly impaired for the C110S and C111S mutants at all cadmium concentrations up to inhibitory levels, whereas Pb^{II}-responsiveness appeared unaffected (Fig. 7B). Equivalent findings were also obtained using minimal (Sauton) medium (Fig. 8) which reveal no significant reduction in the magnitude of derepression by Pb^{II} in the C110S and C111S mutants, compared to wild-type $CmtR^{Sc}$, whereas Cd^{II}-responsiveness is substantially reduced. These results, when considered in the context of the metal binding properties of wild-type and C110G/C111S $CmtR^{Sc}$, reveal that coordination to metal site 2 in $CmtR^{Sc}$ is required for full transcriptional derepression by Cd^{II} in the cell. In contrast, Pb^{II} is a less potent inducer of *cmt-lacZ* expression *in vivo* and does not require metal site 2 for this activity.

DISCUSSION

$CmtR^{Sc}$ (SCO0875) is a *M. tuberculosis* CmtR homolog in *S. coelicolor* that shares 52% sequence identity with $CmtR^{Mtb}$. *S. coelicolor* belongs to the same taxonomic order (Actinomycetales) as the causative agents of tuberculosis and leprosy (*M. tuberculosis and M. leprae*), but is a soil-dwelling bacterium that may more often encounter heavy metal polluted environments (14). However, *M. tuberculosis* is also suggested to encounter heavy metal ions such as Cd^{II} due to their accumulation in alveolar macrophages as a result of air pollution and cigarette smoking (9). As a result, metal-specific regulatory machinery is required to manage the intracellular concentrations of these ions (1). *M. tuberculosis* CmtR is the founding member of a subfamily of winged helical DNA-binding repressors from the ArsR metal-sensing family that employ characteristic α4C metal sites that respond selectively to Cd^{II} and Pb^{II} (6–8). A search of $CmtR^{Mtb}$ homologs in *S. coelicolor* identified two nearly identical open reading frames (locus tags SCO0875 and SCO3522) that appear to encode a $CmtR^{Sc}$ that differ by just ten amino acids, and immediately upstream of ORFs that encode what are predicted to be nearly identical cation diffusion facilitator (CDF) family heavy metal transporters. The presence of what would appear to be two functionally redundant operons may well reflect the need for *S. coelicolo*r to rapidly sense and efflux (or otherwise detoxify) any Cd^{II} and Pb^{II} encountered in the environment.

In this study, we chose the gene encoded by locus tag SCO0875 as representative of $CmtR^{Sc}$ for detailed study and comparison with $CmtR^{Mtb}$. We were particularly intrigued by the presence of two C-terminal vicinal cysteines in $CmtR^{Sc}$, Cys110 and Cys111, both of which are conserved in SCO0875 and SCO3522. Substitution of these residues with non-liganding residues was expected to yield a regulator that behaves much like wild-type $CmtR^{Mtb}$. *In vitro* metal titration experiments confirm this, but also reveal a second metal site in $CmtR^{Sc}$ which is formed by Cys-S^{-} coordination bonds donated by Cys110, Cys111 and a third as yet unidentified ligand. Cys24, which is at least partly exposed to solvent in the solution structure of Cd^{II}-bound CmtR (Fig. 1B) (8) could readily complete an S_3 or $S_3(O)$ coordination complex. Since the solution structural model of Cd^{II}-bound CmtR ends at Arg106, this suggests that the C-terminal tail is highly flexible; if so, inspection of this structure suggests that the C-terminal Cys110/Cys111 pair of one subunit could potentially come in close physical proximity of Cys24 in the α2 helix of the same subunit by crossing over the “front” of the molecule in the orientation shown in Fig. 1B. In this case however Cys24 can *not* function as a key regulatory residue since *in vivo* β-galactosidase assays reveal that substitution of Cys24 does not influence Cd^{II} responsiveness of $CmtR^{Sc}$ in contrast to Cys110 and Cys111; a similar finding characterizes the primary α4C metal site in C24S $CmtR^{Mtb}$ (6). Cys24 may still complete the coordination structure of metal site 2, but it may simply increase the affinity of the site for Cd^{II} rather than function as an allosteric residue (23), much like that found previously for His100 in the Zn^{II} sensor *S. aureus* CzrA (42) and the Cys7 and Cys58 of the S_4 Cd^{II} sensor *S. aureus* pI258 CadC (12). Other non-thiolate possibilities for the third ligand are of course formally possible, but would not be compatible with the absorption spectroscopy of the Cd^{II} and Pb^{II} complexes (12). Detailed structural or ^{113}Cd NMR studies (7,12,32) will be required to further elucidate the coordination structure of metal site 2 in $CmtR^{Sc}$.

$CmtR^{Sc}$ displays an *in vivo* metal specificity for Cd^{II} and Pb^{II} that is identical to that of $CmtR^{Mtb}$ in the heterologous host *M. smegmatis*; given the similarity of these two bacterial species, these findings suggest that $CmtR^{Sc}$ is a *bona fide* Cd^{II}/Pb^{II} sensor in *S. coelicolor*. Although both $CmtR^{Sc}$ and $CmtR^{Mtb}$ share the same primary allosteric α4C metal site with the Hg^{II} sensor MerR in *Streptomyces lividans* (43), neither CmtR senses Hg^{II} in *M. smegmatis* (7). In addition, neither $CmtR^{Sc}$- nor $CmtR^{Mtb}$-repressed transcription is inducible by Zn^{II} (7), despite the fact that each retains the ability to bind Zn^{II} *in vitro* (7).

Little is known about how *Streptomyces spp*. handle Hg^{II} toxicity and how this might differ from *Mycobacteria*; as a result, it is formally possible that in addition to detecting Cd^{II} and Pb^{II}, $CmtR^{Sc}$ may detect Hg^{II} in the native host. A more important issue is how CmtRs sense Cd^{II} and Pb^{II} over Zn^{II} in the cell. Although absolute metal affinity of the sensing sites may not fully explain metal selectivity in the cell, this simple explanation may be at least partially operative here. Both proteins have Zn^{II} affinity $\leq 10^{10}$ M^{-1}, which is three orders less than the affinity for Cd^{II} (Fig. 3) (7) which itself is comparable to that previously measured K_{Cd} for the Cd^{II}/Pb^{II} sensor CadC (27). Furthermore, a $K_{Zn} \leq 10^{10}$ M^{-1} may not be sufficient to be detected in cells by CmtR, since the typical bacterial Zn^{II} sensor is characterized by an equilibrium affinity for Zn^{II} in the 10^{12}–10^{15} M^{-1} range. In fact, a protein encoded by locus tag SCO6459 is a strong candidate α5 site zinc sensor in *S. coelicolor* that may be poised to detect weakly chelated Zn^{II} buffered in the 10^{-12} to 10^{-15} M range (29,42,44,45). This ensures that both *cmtR*^{Sc}*-sco0874* and *sco3522-sco3521* operons will be induced by Cd^{II} and Pb^{II} and not by Zn^{II} so that these toxic metals can be selectively effluxed from the cytosol.

The primary α4C metal site 1 is necessary for both Cd^{II} and Pb^{II} detection in the cell, but is not sufficient for full Cd^{II} responsiveness, which clearly requires coordination by metal site 2 (Figs. 7–8). The evolutionary advantage of this to *S. coelicolor* is unknown, but may reflect the possibility that Cd^{II} salts and low molecular weight complexes are far more bioavailable (soluble) in soils than Pb^{II} complexes (which may be readily precipitated) and thus must be more efficiently detoxified. Clearly, Cd^{II} is a stronger inducer of $CmtR^{Sc}$-mediated transcriptional derepression in *M. smegmatis* than is Pb^{II} over a similar concentration range of added metal, and most of this difference can be traced to Cd^{II} occupancy of metal site 2 (Figs. 6–7). Pb^{II}, being the larger cation, may well fail to induce the same change in homodimer structure and/or dynamics that has been shown to be important in $CmtR^{Mtb}$ (8) and other ArsR family sensors (46). Alternatively, the bioavailable concentration of Pb^{II} achievable in *M. smegmatis* at the maximum permissive concentration of this cation (≈5 mM; Figs. 7–8) may not high enough to fill metal site 2 in the *M. smegmatis* cytosol; as a result, $CmtR^{Sc}$ is a poorer Pb^{II} sensor *in vivo*. In any case, filling both metal sites in $CmtR^{Sc}$ may well stabilize the allosterically inhibited low-affinity DNA binding state beyond that which can be achieved by filling the pair of primary α4C metal sites alone. Indeed, previous quantitative DNA binding experiments reveal that Cd^{II} is a relative poorer allosteric negative inhibitor of $CmtR^{Mtb}$ binding to DNA relative to other ArsR-family metalloregulatory proteins (1,11); this suggests that Cd^{II} binding to metal site 2 may further enhance allosteric regulation of DNA binding in a way that leads to increased transcription derepression in the cell. Alternatively or in addition, the second high affinity ($K_{Cd} \geq 10^{12}$ M^{-1}) cadmium binding site on $CmtR^{Sc}$ may also simply allow *S. coelicolor* to sequester (chelate) more Cd^{II} under conditions of Cd^{II} stress once $CmtR^{Sc}$ is dissociated from its DNA operator. Understanding the structural and physiological role of metal site 2 in $CmtR^{Sc}$ requires further investigation.

$CmtR^{Sc}$ is not the first ArsR family regulator with two structurally distinct pairs of metalloregulatory sites per dimer. Other examples include the Cd^{II}/Pb^{II} sensor pI258 CadC (12) and Cu^{I} sensor *O. brevis* BxmR (11). CadC employs four conserved Cys in Cd^{II}, Co^{II} and Bi^{III} binding while adopting an S_3 coordination complex with Pb^{II} in its primary α3N metal site; Zn^{II} binding to a pair of C-terminal interhelical α5 sites is functionally silent in CadCs, while other CadCs and α3N-type sensors have dispensed with this site entirely (12,47). In BxmR, the α3N site is a major sensing site for Cd^{II} and Cu^{I}, the latter of which forms a binuclear $Cu^{I}_2S_4$ cluster (11); a C-terminal α5 site has evolved exclusively for Zn^{II} sensing. Thus, in the case of BxmR, the presence of two distinct metal sites relaxes the metal selectivity of this particular sensor. In $CmtR^{Sc}$, the impact of metal site 2 on $CmtR^{Sc}$ function largely parallels the situation in CadCs, where the secondary site does not change

the metal specificity profile of the primary metal site (12,48), but unlike in CadCs, enhances its effectiveness in the cell.

Finally, $CmtR^{Sc}$ is the first ArsR family metal sensor to be characterized from *S. coelicolor* and is shown here to possess both a metal sensing site anticipated on the basis of its classification as an CmtR-like α4C Pb^{II}/Cd^{II} sensor, as well as a second novel metalloregulatory site not found in other CmtRs. In fact, the presence of consecutive or vicinal Cys residues in what are predicted to be flexible or unstructured N-terminal or C-terminal "tails" like that in metal site 2 in $CmtR^{Sc}$, have previously been shown to function as As^{III} ligands in two arsenic-specific ArsR family proteins recently characterized (49,50); given this, it seemed possible that Cys110 and/or Cys111 might confer a As^{III} sensing function on the Pb^{II}/Cd^{II} sensing CmtR. Our data reveal that this is clearly not the case, at least as measured by transcriptional derepression in *M. smegmatis* (Fig. 6). These findings are consistent with the idea that ArsR family sensors may well be readily classified into subfamilies of paralogs that detect distinct cellular inducers solely on the basis of well-characterized primary structural motifs, rather than global sequence similarity (1,10). However, these core characteristics can be modulated by additional or altogether novel metal sites capable of tuning inducer responsiveness appropriate for the microenvironmental niche in which an organism resides (11,49).

Acknowledgments

This work was supported, in whole or in part, by grants from the National Institutes of Health (GM042569 to D. P. G.) and the Biotechnology and Biological Sciences Research Council (BBSRC) (BB/G010765/1 to J. S. C.)

REFERENCES

1. Ma Z, Jacobsen FE, Giedroc DP. Coordination chemistry of bacterial metal transport and sensing. Chem Rev. 2009; 109:4644–4681. [PubMed: 19788177]
2. Nies DH. Heavy metal-resistant bacteria as extremophiles: molecular physiology and biotechnological use of Ralstonia sp. CH34. Extremophiles. 2000; 4:77–82. [PubMed: 10805561]
3. Schnappinger D, Ehrt S, Voskuil MI, Liu Y, Mangan JA, Monahan IM, Dolganov G, Efron B, Butcher PD, Nathan C, Schoolnik GK. Transcriptional Adaptation of Mycobacterium tuberculosis within Macrophages: Insights into the Phagosomal Environment. J Exp Med. 2003; 198:693–704. [PubMed: 12953091]
4. Payne JC, ter Horst MA, Godwin HA. Lead fingers: Pb^{2+} binding to structural zinc-binding domains determined directly by monitoring lead-thiolate charge-transfer bands. J. Am. Chem. Soc. 1999; 121:6850–6855.
5. Warren MJ, Cooper JB, Wood SP, Shoolingin-Jordan PM. Lead poisoning, haem synthesis and 5-aminolaevulinic acid dehydratase. Trends Biochem Sci. 1998; 23:217–221. [PubMed: 9644976]
6. Cavet JS, Graham AI, Meng W, Robinson NJ. A cadmium-lead-sensing ArsR-SmtB repressor with novel sensory sites. Complementary metal discrimination by NmtR and CmtR in a common cytosol. J. Biol. Chem. 2003; 278:44560–44566. [PubMed: 12939264]
7. Wang Y, Hemmingsen L, Giedroc DP. Structural and functional characterization of Mycobacterium tuberculosis CmtR, a PbII/CdII-sensing SmtB/ArsR metalloregulatory repressor. Biochemistry. 2005; 44:8976–8988. [PubMed: 15966722]
8. Banci L, Bertini I, Cantini F, Ciofi-Baffoni S, Cavet JS, Dennison C, Graham AI, Harvie DR, Robinson NJ. NMR structural analysis of cadmium sensing by winged helix repressor CmtR. J. Biol. Chem. 2007; 282:30181–30188. [PubMed: 17599915]
9. Chauhan S, Kumar A, Singhal A, Tyagi JS, Krishna Prasad H. CmtR, a cadmium-sensing ArsR-SmtB repressor, cooperatively interacts with multiple operator sites to autorepress its transcription in Mycobacterium tuberculosis. FEBS J. 2009; 276:3428–3439. [PubMed: 19456862]
10. Campbell DR, Chapman KE, Waldron KJ, Tottey S, Kendall S, Cavallaro G, Andreini C, Hinds J, Stoker NG, Robinson NJ, Cavet JS. Mycobacterial cells have dual nickel-cobalt sensors: sequence

relationships and metal sites of metal-responsive repressors are not congruent. J. Biol. Chem. 2007; 282:32298–32310. [PubMed: 17726022]

11. Liu T, Chen X, Ma Z, Shokes J, Hemmingsen L, Scott RA, Giedroc DP. A Cu(I)-sensing ArsR family metal sensor protein with a relaxed metal selectivity profile. Biochemistry. 2008; 47:10564–10575. [PubMed: 18795800]
12. Busenlehner LS, Weng TC, Penner-Hahn JE, Giedroc DP. Elucidation of primary (α3N) and vestigial (α5) heavy metal-binding sites in *Staphylococcus aureus* pI258 CadC: evolutionary implications for metal ion selectivity of ArsR/SmtB metal sensor proteins. J. Mol. Biol. 2002; 319:685–701. [PubMed: 12054863]
13. Ye J, Kandegedara A, Martin P, Rosen BP. Crystal structure of the Staphylococcus aureus pI258 CadC Cd(II)/Pb(II)/Zn(II)-responsive repressor. J. Bacteriol. 2005; 187:4214–4221. [PubMed: 15937183]
14. Bentley SD, Chater KF, Cerdeno-Tarraga AM, Challis GL, Thomson NR, James KD, Harris DE, Quail MA, Kieser H, Harper D, Bateman A, Brown S, Chandra G, Chen CW, Collins M, Cronin A, Fraser A, Goble A, Hidalgo J, Hornsby T, Howarth S, Huang CH, Kieser T, Larke L, Murphy L, Oliver K, O'Neil S, Rabbinowitsch E, Rajandream MA, Rutherford K, Rutter S, Seeger K, Saunders D, Sharp S, Squares R, Squares S, Taylor K, Warren T, Wietzorrek A, Woodward J, Barrell BG, Parkhill J, Hopwood DA. Complete genome sequence of the model actinomycete Streptomyces coelicolor A3(2). Nature. 2002; 417:141–147. [PubMed: 12000953]
15. Borodina I, Krabben P, Nielsen J. Genome-scale analysis of Streptomyces coelicolor A3(2) metabolism. Genome Res. 2005; 15:820–829. [PubMed: 15930493]
16. Wagner D, Maser J, Lai B, Cai Z, Barry CE 3rd, Honer Zu Bentrup K, Russell DG, Bermudez LE. Elemental analysis of Mycobacterium avium-, Mycobacterium tuberculosis-, and Mycobacterium smegmatis-containing phagosomes indicates pathogen-induced microenvironments within the host cell's endosomal system. J. Immunol. 2005; 174:1491–1500. [PubMed: 15661908]
17. Collins HL. Withholding iron as a cellular defence mechanism--friend or foe? Eur. J. Immunol. 2008; 38:1803–1806. [PubMed: 18546145]
18. White C, Lee J, Kambe T, Fritsche K, Petris MJ. A role for the ATP7A copper-transporting ATPase in macrophage bactericidal activity. The Journal of biological chemistry. 2009; 284:33949–33956. [PubMed: 19808669]
19. Techau ME, Valdez-Taubas J, Popoff JF, Francis R, Seaman M, Blackwell JM. Evolution of differences in transport function in Slc11a family members. J Biol Chem. 2007; 282:35646–35656. [PubMed: 17932044]
20. An YJ, Ahn BE, Han AR, Kim HM, Chung KM, Shin JH, Cho YB, Roe JH, Cha SS. Structural basis for the specialization of Nur, a nickel-specific Fur homolog, in metal sensing and DNA recognition. Nucleic Acids Res. 2009:3442–3451. [PubMed: 19336416]
21. Ahn BE, Cha J, Lee EJ, Han AR, Thompson CJ, Roe JH. Nur, a nickel-responsive regulator of the Fur family, regulates superoxide dismutases and nickel transport in Streptomyces coelicolor. Mol. Microbiol. 2006; 59:1848–1858. [PubMed: 16553888]
22. Shin JH, Oh SY, Kim SJ, Roe JH. The zinc-responsive regulator Zur controls a zinc uptake system and some ribosomal proteins in Streptomyces coelicolor A3(2). J Bacteriol. 2007; 189:4070–4077. [PubMed: 17416659]
23. Giedroc DP, Arunkumar AI. Metal sensor proteins: nature's metalloregulated allosteric switches. Dalton Trans. 2007; 29:3107–3120. [PubMed: 17637984]
24. Montanini B, Blaudez D, Jeandroz S, Sanders D, Chalot M. Phylogenetic and functional analysis of the Cation Diffusion Facilitator (CDF) family: improved signature and prediction of substrate specificity. BMC Genomics. 2007; 8:107. [PubMed: 17448255]
25. Guo J, Giedroc DP. Zinc site redesign in T4 gene 32 protein: structure and stability of cobalt(II) complexes formed by wild-type and metal ligand substitution mutants. Biochemistry. 1997; 36:730–742. [PubMed: 9020770]
26. Tan X, Kagiampakis I, Surovtsev IV, Demeler B, Lindahl PA. Nickel-dependent oligomerization of the alpha subunit of acetyl-coenzyme a synthase/carbon monoxide dehydrogenase. Biochemistry. 2007; 46:11606–11613. [PubMed: 17887777]

27. Busenlehner LS, Cosper NJ, Scott RA, Rosen BP, Wong MD, Giedroc DP. Spectroscopic properties of the metalloregulatory Cd(II) and Pb(II) sites of *S. aureus* pI258 CadC. Biochemistry. 2001; 40:4426–4436. [PubMed: 11284699]
28. Martell, AE.; Smith, RM. Critical Stability Constants. Plenum Press; New York: 1979–1989.
29. VanZile ML, Chen X, Giedroc DP. Structural characterization of distinct α3N and α5 metal sites in the cyanobacterial zinc sensor SmtB. Biochemistry. 2002; 41:9765–9775. [PubMed: 12146942]
30. Timm J, Lim EM, Gicquel B. Escherichia coli-mycobacteria shuttle vectors for operon and gene fusions to lacZ: the pJEM series. Journal of bacteriology. 1994; 176:6749–6753. [PubMed: 7961429]
31. Cavet JS, Meng W, Pennella MA, Appelhoff RJ, Giedroc DP, Robinson NJ. A nickel-cobalt-sensing ArsR-SmtB family repressor. Contributions of cytosol and effector binding sites to metal selectivity. J Biol Chem. 2002; 277:38441–38448. [PubMed: 12163508]
32. Matzapetakis M, Farrer BT, Weng TC, Hemmingsen L, Penner-Hahn JE, Pecoraro VL. Comparison of the binding of cadmium(II), mercury(II), and arsenic(III) to the de novo designed peptides TRI L12C and TRI L16C. J. Am. Chem. Soc. 2002; 124:8042–8054. [PubMed: 12095348]
33. Pountney DL, Tiwari RP, Egan JB. Metal- and DNA-binding properties and mutational analysis of the transcription activating factor, B, of coliphage 186: a prokaryotic C4 zinc-finger protein. Protein Sci. 1997; 6:892–902. [PubMed: 9098899]
34. Henehan CJ, Pountney DL, Zerbe O, Vasak M. Identification of cysteine ligands in metalloproteins using optical and NMR spectroscopy: cadmium-substituted rubredoxin as a model [Cd(CysS)4]2-center. Protein Sci. 1993; 2:1756–1764. [PubMed: 8251947]
35. Claudio ES, Magyar JS, Godwin HA. Prog. Inorg. Chem. 2003; 51:1–144.
36. Magyar JS, Weng TC, Stern CM, Dye DF, Rous BW, Payne JC, Bridgewater BM, Mijovilovich A, Parkin G, Zaleski JM, Penner-Hahn JE, Godwin HA. Reexamination of lead(II) coordination preferences in sulfur-rich sites: implications for a critical mechanism of lead poisoning. J Am Chem Soc. 2005; 127:9495–9505. [PubMed: 15984876]
37. Gamelin DRR, D. W. Hay MT, Houser RP, Mulder TC, Canters GW, de Vries S, Tolman WB, Lu Y, Solomon EI. Spectroscopy of mixed-valence CuA-type centers: Ligand-field control of ground-state properties related to electron transfer. J. Am. Chem. Soc. 1998; 120:5246–5263.
38. Basumallick LG, S. D. Randall DW, Hedman B, Hodgson KO, Fujisawa K, Solomon EI. Spectroscopic comparison of the five-coordinate [Cu(SMeIm)(HB(3,5-iPr2pz)3)] with the four-coordinate [Cu(SCPh3)(HB(3,5-iPr2pz)3)]: effect of coordination number increase on a blue copper type site. Inorg. Chim. Acta. 2002; 337:357–365.
39. Lever ABP. J. Chem. Educ. 1974; 51:612–616.
40. Hernandez-Abanto SM, Woolwine SC, Jain SK, Bishai WR. Tetracycline-inducible gene expression in mycobacteria within an animal host using modified Streptomyces tcp830 regulatory elements. Arch Microbiol. 2006; 186:459–464. [PubMed: 16944099]
41. Raghunand TR, Bishai WR. Mapping essential domains of Mycobacterium smegmatis WhmD: insights into WhiB structure and function. J Bacteriol. 2006; 188:6966–6976. [PubMed: 16980499]
42. Pennella MA, Arunkumar AI, Giedroc DP. Individual metal ligands play distinct functional roles in the zinc sensor Staphylococcus aureus CzrA. J. Mol. Biol. 2006; 356:1124–1136. [PubMed: 16406068]
43. Rother D, Mattes R, Altenbuchner J. Purification and characterization of MerR, the regulator of the broad-spectrum mercury resistance genes in Streptomyces lividans 1326. Mol Gen Genet. 1999; 262:154–162. [PubMed: 10503547]
44. Outten CE, O'Halloran TV. Femtomolar sensitivity of metalloregulatory proteins controlling zinc homeostasis. Science. 2001; 292:2488–2492. [PubMed: 11397910]
45. Waldron KJ, Robinson NJ. How do bacterial cells ensure that metalloproteins get the correct metal? Nat Rev Microbiol. 2009; 7:25–35. [PubMed: 19079350]
46. Arunkumar AI, Campanello GC, Giedroc DP. Solution structure of a paradigm ArsR family zinc sensor in the DNA-bound state. Proc Natl Acad Sci USA. 2009; 106:18177–18182. [PubMed: 19822742]

47. Liu T, Golden JW, Giedroc DP. A zinc(II)/lead(II)/cadmium(II)-inducible operon from the cyanobacterium Anabaena is regulated by AztR, an α3N ArsR/SmtB metalloregulator. Biochemistry. 2005; 44:8673–8683. [PubMed: 15952774]

48. Kandegedara A, Thiyagarajan S, Kondapalli KC, Stemmler TL, Rosen BP. Role of bound Zn(II) in the CadC Cd(II)/Pb(II)/Zn(II)-responsive repressor. J. Biol. Chem. 2009; 284:14958–14965. [PubMed: 19286656]

49. Ordoñez E, Thiyagarajan S, Cook JD, Stemmler TL, Gil JA, Mateos LM, Rosen BP. Evolution of metal(loid) binding sites in transcriptional regulators. J. Biol. Chem. 2008; 283:25706–25714. [PubMed: 18591244]

50. Qin J, Fu HL, Ye J, Bencze KZ, Stemmler TL, Rawlings DE, Rosen BP. Convergent evolution of a new arsenic binding site in the ArsR/SmtB family of metalloregulators. J. Biol. Chem. 2007; 282:34346–34355. [PubMed: 17897948]

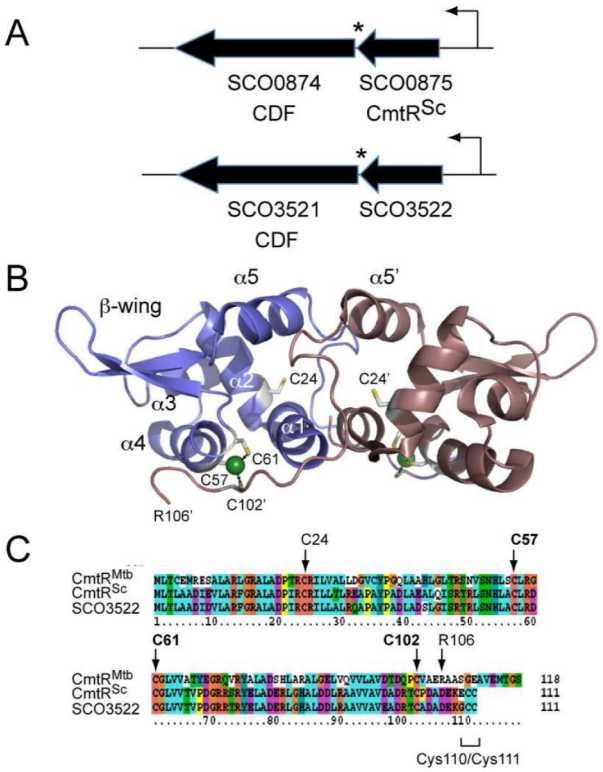

Figure 1. Genomic region of CmtR homologs in *S. coelicolor*, solution structure and multiple sequence alignment of *M. tuberculosis* CmtR

(A) Genomic region around *S. coelicolor* $CmtR^{Sc}$ (SCO0875) and SCO3522; each gene is separated by a single TGA termination codon (*) from homologous downstream genes SCO0874 and SCO3521 that encode putative CDF-family heavy metal transporters. The surrounding genomic regions are completely unrelated in the two loci. (B) Ribbon diagram of the solution structure of the *M. tuberculosis* CmtR-Cd^{II} complex (2jsc) with individual protomers shaded *slate* and *violet* and the two symmetry-related Cd^{II} ions colored *green* (8). The secondary structural units are labeled, with the side-chains of C24 and the Cd^{II}-coordinating residues, C57, C61 and C102' (prime designation, opposite subunit) highlighted in *stick*. The most C-terminal residue in the structural model of each protomer is R106. (C) Multiple sequence alignment of $CmtR^{Mtb}$, $CmtR^{Sc}$ and the product of SCO3522. Cd^{II}-coordinating residues in $CmtR^{Mtb}$ are highlighted in ***bold***, with other residues as in panel B.

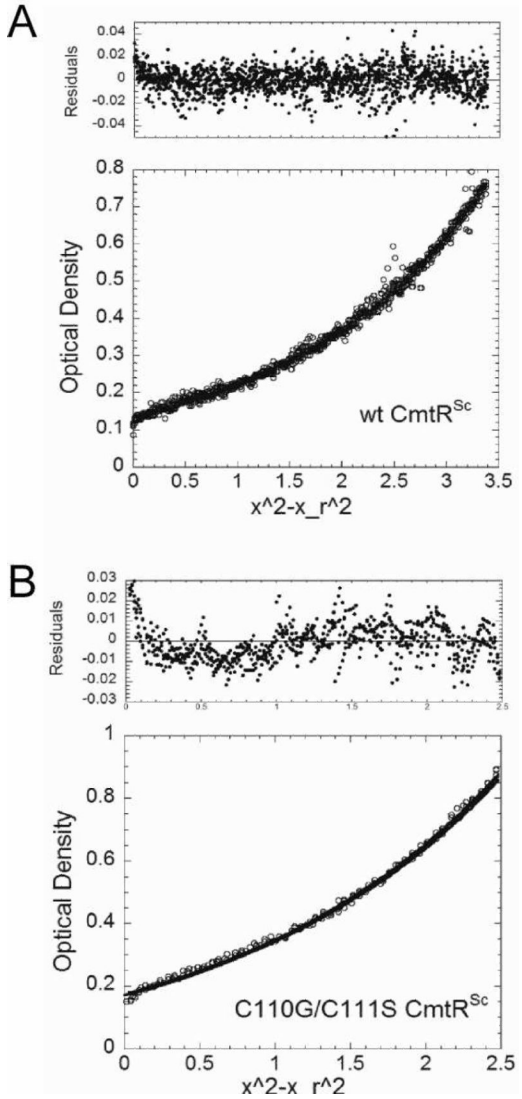

Figure 2. Analytical sedimentation equilibrium ultracentrifugation of CmtR^{Sc} and C110G/C111S CmtR^{Sc}

(A) 5.03 μM monomer wild-type CmtR^{Sc}. (B) 8.0 μM monomer C110G/C111S CmtR^{Sc}. Filled symbols in upper panels represent an overlay of data collected during the last seven scans and indicate that equilibrium had been reached. The solid line represents the global simultaneous fit for a single ideal species model using Ultrascan. For wild-type CmtR^{Sc}, the fitted M_w is 23,820 Da (theoretical dimer M_w = 24,378 Da), variance = 1.0689 e^{-4}. For C110G/C111S CmtR^{Sc}, the fitted M_w is 25,690 Da (theoretical dimer M_w = 24,252 Da), variance = 5.8026 e^{-5}. Conditions: 10 mM Hepes, 0.4 M NaCl, and 0.1 mM EDTA at pH 7.0, 25.0 °C, and 20,000 rpm rotor speed.

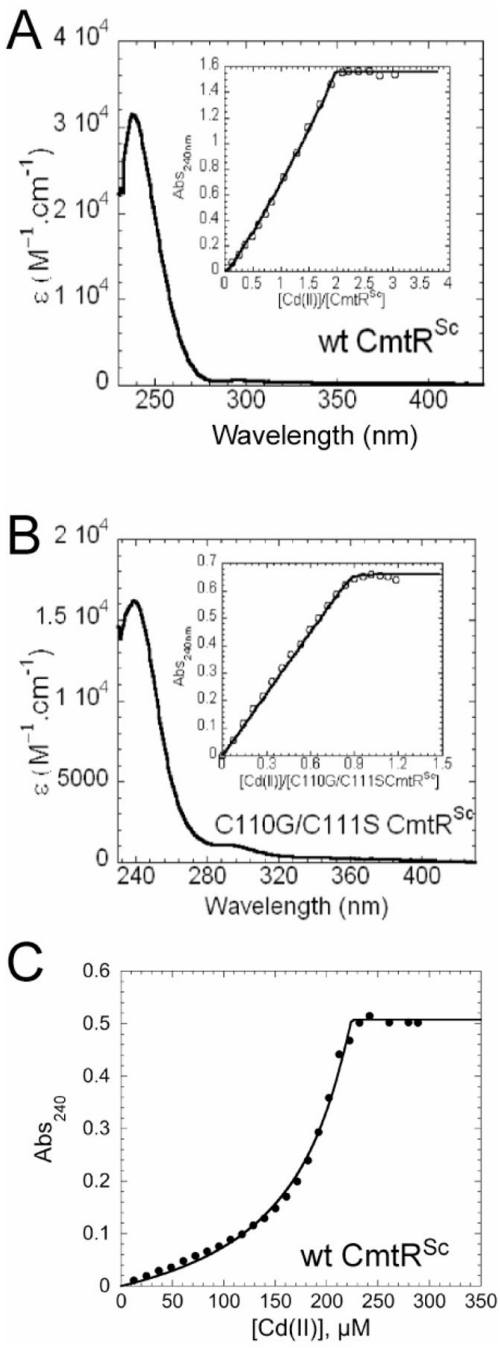

Figure 3. Cd^{II} titrations of wild-type and C110G/C111S $CmtR^{Sc}$

(A) Apoprotein subtracted difference spectrum of wild-type $CmtR^{Sc}$ (50.7 μM monomer). (B) Apoprotein subtracted difference spectrum of C110G/C111S $CmtR^{Sc}$ (44.8 μM monomer). $CmtR^{Sc}$ variants were titrated anaerobically with increasing concentrations of Cd^{II}. *Inset*, Cd^{II} binding isotherm plotted as change in A_{240} vs. [$CmtR^{Sc}$ variant monomer]. (C) Cd^{II}-EDTA competition binding isotherm in which 20.9 μM wild-type $CmtR^{Sc}$ was titrated with Cd^{II} in the presence of 227 μM EDTA. Conditions: 10 mM Hepes, 0.4 M NaCl, pH 7.0, 25°C.

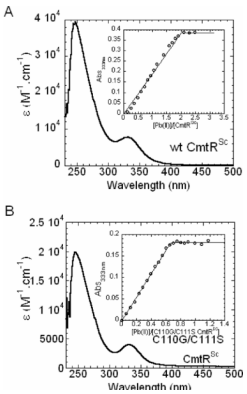

Figure 4. Pb^{II} titrations of $CmtR^{Sc}$ and C110G/C111S $CmtR^{Sc}$

(A) Apoprotein subtracted difference spectrum of wild-type $CmtR^{Sc}$ (50.8 μM). (B) Apoprotein subtracted difference spectrum of C110G/C111S $CmtR^{Sc}$ (53.7 μM). $CmtR^{Sc}$ variants were titrated anaerobically with increasing concentrations of Pb^{II}. *Inset*, Pb^{II} binding isotherm plotted as change in A_{333} vs. [$CmtR^{Sc}$ variant monomer] Conditions: 10 mM Bis-Tris, 0.4 M NaCl, pH 7.0, 25.0 °C.

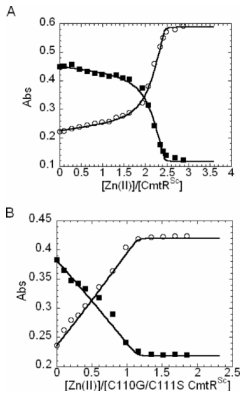

Figure 5. Zn^{II} titrations of $CmtR^{Sc}$ and C110G/C111S $CmtR^{Sc}$ using magfura-2 as an indicator

(A) 30 μM $CmtR^{Sc}$ and 14.7 μM magfura-2 and (B) 30 μM C110G/C111S $CmtR^{Sc}$ and 15 μM magfura-2 were present. The empty circles represent A_{325} and the filled squares represent A_{366}. The solid line represents a global non-linear least square fit to a model that incorporates the stepwise binding of two Zn^{II} (defined by K_{PZn} and K_{PZn2}) to a $CmtR^{Sc}$ monomer using Dynafit. The titration for C110G/C111S $CmtR^{Sc}$ was fitted using one Zn^{II} to protein monomer binding model. The following parameters were obtained for wild-type $CmtR^{Sc}$: $K_{PZn} = 5.3\ (\pm 1.8) \times 108\ M^{-1}$ (a lower limit under these conditions), $K_{PZn2} = 6.7\ (\pm 1.4) \times 10^8\ M^{-1}$. For C110G/C111S $CmtR^{Sc}$, $K_{PZn} = 5.5\ (\pm 1.2) \times 10^7\ M^{-1}$. Conditions: 10 mM Hepes, 0.4 M NaCl at pH 7.0 and 25.0 °C.

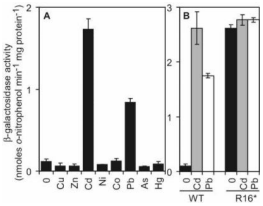

Figure 6. CmtR^{Sc} responds to Cd^{II} and Pb^{II} in an actinomycete host

(A) β-galactosidase activity measured in *M. smegmatis* mc^{2}155 containing *cmtR^{Sc}* and its operator-promoter region fused to *lacZ* following growth in LB medium with no metal supplement or with maximum permissive concentrations of Zn^{II} (100 μM), Co^{II} (200 μM), Ni^{II} (500 μM), Cd^{II} (7.5 μM), Cu^{II} (500 μM), Pb^{II} (3.75 μM), As^{III}(20 μM), or Hg^{II} (0.025 μM). (B) β-galactosidase activity in cells containing wild-type CmtR^{Sc} (*WT*) or the stop codon derivative (*R16**) following growth in LB medium with no metal supplement (*black*) or maximum permissive concentrations of Cd^{II} (*gray*) or Pb^{II} (*white*).

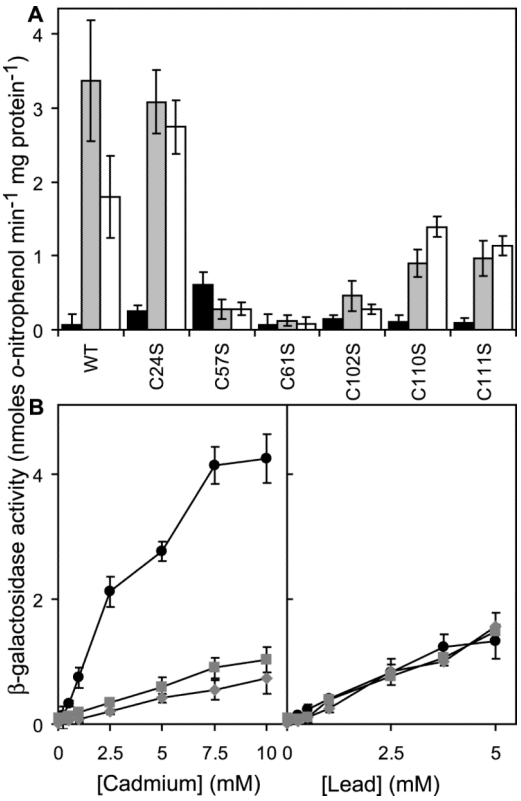

Figure 7. Metal sensing ligands of CmtR^{Sc}

(A) β-galactosidase activity measured in *M. smegmatis* mc^{2}155 containing wild-type CmtR^{Sc} (*WT*) or derivatives with indicated cysteine to serine codon substitutions, following growth in LB medium with no metal supplement (*black*) or maximum permissive concentrations of Cd^{II} (*gray*) or Pb^{II} (*white*). (B) β-galactosidase activity in cells containing wild-type CmtR^{Sc} (*black circles*) or the C110S (*gray squares*) and C111S derivatives (*gray diamonds*) grown in LB with up to inhibitory concentrations of Cd^{II} or Pb^{II}. Data points represent the mean (± SE) for three independent experiments, each performed in triplicate.

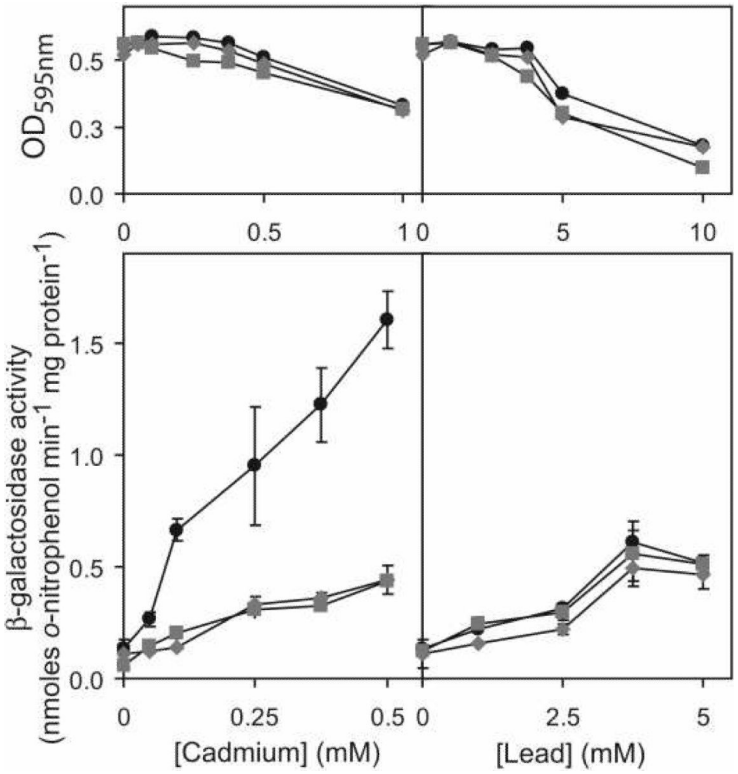

Figure 8. Metal sensing ligands of CmtR^{Sc} as determined on a chemically defined minimal medium

Top panel, Cell viability of *M. smegmatis* mc^{2}155 containing wild-type CmtR^{Sc} (*black circles*), C110S (*gray squares*) and C111S derivatives (*gray diamonds*) grown on minimal Sauton medium (containing 2.9 mM phosphate) as a function of total added Cd^{II} (*left*) or Pb^{II} (*right*). *Lower panel*, β-galactosidase activity in cells containing wild-type CmtR^{Sc} (*black circles*), C110S (*gray squares*) or C111S CmtR^{Sc} (*gray diamonds*) grown in minimal media up to inhibitory concentrations of Cd^{II} or Pb^{II}. Data points represent the mean (± SE) for three independent experiments, each performed in triplicate.